Direct Conversion of Heat to Electricity Using First-Order Phase Transformations in Ferroelectrics

Ashley Bucsek,[1,*] William Nunn,[2,†] Bharat Jalan,[2] and Richard D. James[3,‡]

[1] *Department of Mechanical Engineering, University of Michigan, Ann Arbor, Michigan 48109, USA*
[2] *Department of Chemical Engineering and Materials Science, University of Minnesota, Minneapolis, Minnesota 55455, USA*
[3] *Department of Aerospace Engineering and Mechanics, University of Minnesota, Minneapolis, Minnesota 55455, USA*

(Received 6 May 2019; revised manuscript received 6 July 2019; published 23 September 2019)

There is a growing and drastically underutilized abundance of energy stored on earth at small temperature difference, most familiarly in the form of low-grade waste heat. For the purpose of making use of this stockpile of energy, the direct conversion of heat to electricity is demonstrated using first-order phase transformations in lead-free $BaTiO_3$ ferroelectrics. The thermodynamics of solid-state energy conversion using first-order phase transformations is investigated using a free-energy approach wherein the importance of the well-known Clausius-Clapeyron relation in opening up the mixed-phase region is discussed. A simple two-capacitor circuit is introduced to experimentally demonstrate the direct conversion of heat to electricity. By fluctuating the temperature by just $\pm 5\,^{\circ}\mathrm{C}$, current spikes of roughly 1 μA are sent back and forth across an electric load with no external battery attached. Finally, a supercritical ferroelectric Carnot cycle that would produce an energy density of 1.15 $\mathrm{J/cm^3}$ with a thermal efficiency of 15% is introduced, simulated, and compared with state-of-the-art pyroelectric energy-conversion methods.

DOI: 10.1103/PhysRevApplied.12.034043

I. INTRODUCTION

The functional properties of multiferroic materials have driven them to the forefront of contemporary research areas ranging from energy conversion to sensing to actuation [1–5]. Ferroic materials respond to external stimuli by undergoing spontaneous changes in macroscopic behavior: ferroelastics, ferroelectrics, and ferromagnetics undergo spontaneous changes in elastic, electrical, and magnetic ordering, respectively. Multiferroic materials exhibit two or all of these behaviors, where the discrete ferroic behaviors are often coupled. In a subset of multiferroic materials, the functional properties are enabled via diffusionless first-order phase transformations where sharp changes in lattice structure are coupled with sharp changes in elastic, electrical, or magnetic properties.

For example, ferroelastic-ferroelectric $BaTiO_3$ undergoes a first-order phase transformation from a paraelectric cubic phase to a strongly ferroelectric tetragonal phase upon cooling. When this transformation is induced while the material is under an electrical bias, it results in a jump in polarization ($> 15\ \mathrm{C/m^2}$) [6]. The first-order nature of the phase transformation not only makes this change in properties abrupt, but it also gives rise to a mixed-phase region that can potentially support high-efficiency thermodynamic cycles [7]. This is the solid-state analog of the utility of first-order phase transformations in steam generators. $BaTiO_3$ has other advantages as well: it is free of toxic and environmentally hazardous lead [8,9], has a low Curie temperature ($T_c = 120 - 130\,^{\circ}\mathrm{C}$) [10–12], and has relatively low hysteresis [13,14]. This combination of properties makes this well-studied oxide a natural fit for the conversion of energy stored at small temperature differences to electricity.

Energy stored at small temperature difference is a growing and drastically underutilized stockpile of convertible resources. According to a 2008 U.S. Department of Energy report on waste heat recovery, the U.S. industrial sector alone consumes one fifteenth of the power consumed from all sources worldwide: 25%–50% of this power is rejected as waste heat and 60% of unrecovered waste heat is "low grade" or "low quality" ($< 200^{\circ}\mathrm{C}$) [15]. A more recent 2016 study on energy consumption in the U.S. reports that two thirds of all of the energy produced in the U.S. is now ultimately rejected as waste heat [16]. Besides the massive reserves of waste heat from man-made sources, there are also enormous natural reserves stored on earth at small temperature difference, such as

*ashley.n.bucsek@gmail.com
†nunnx029@umn.edu
‡james@umn.edu

the heat stored in large bodies of water. Other significant sources in the small-temperature-difference regime include the heat generated by solar-thermal plants and the growing waste heat from data centers, which in the U.S. now consume about 3% of the energy budget. For the latter, chip-level integration is desirable and possible with the method discussed here.

Energy conversion using first-order phase transformations between ferromagnetic and nonferromagnetic phases, or ferroelectric and nonferroelectric phases, has been discussed in Refs. [7,17,18]. To recover the electricity, one uses induction in the magnetic case and capacitance in the ferroelectric case. In the ferroelectric case studied in this paper, a critical role is played by the well-known effect of the electric field on the transformation temperature. In the energy-conversion device, this effect serves to split the transformation temperature so that the transformation occurs at a higher temperature on heating and a lower temperature on cooling, opening up the mixed-phase region referred to above. While the optimization is different, a relevant literature for ferroelectric energy conversion is the modeling of electrocaloric refrigeration [19]: ferroelectric energy conversion can be considered as electrocaloric cycles run backward.

These effects distinguish the method discussed here from the pyroelectric methods, such as those discussed in Refs. [5,20–26]. Pyroelectricity is a single-phase effect governed by the pyroelectric coefficients. For the analysis of the latter, one uses the Maxwell relations, while the splitting of transformation temperature mentioned above is governed by the well-known Clausius-Clapeyron equation, based on a free energy that contains a polarization dependence (see below). However, if a first-order ferroelectric phase transformation is smeared out by inhomogeneity and disorder at the nanoscale, such as in a relaxor ferroelectric, then it can appear to behave like a single-phase material; this is exploited in Refs. [5,22–24]. Exactly the same smearing occurs in magnetic materials and has led to controversy as to whether the magnetocaloric effect should be modeled as a first-order transformation or as a single-phase material; this was resolved in Ref. [27]. In the present paper, in both theory and experiment, we exploit the first-order nature of the phase transformation.

For the evaluation of the performance of a heat-to-electricity energy conversion device, it is essential to distinguish the cases of generator efficiency and system efficiency. Losses in the generator itself can be compensated by periodic replenishing ("priming") and this can be effective in optimizing the efficiency or power output [28,29], as in our analysis of the supercritical ferroelectric Carnot cycle below. However, overall measures of performance, such as system efficiency, that can be used to compare different energy-conversion devices must account accurately for all sources of power, such as depletion of batteries, in addition to the heat source and must assure that the device returns to its original state after each cycle [7].

In this paper, we examine the thermodynamics of solid-state energy conversion using first-order phase transformations in $BaTiO_3$. We give a detailed model of the process based on a Landau-type free energy [6]. We demonstrate the conversion of small temperature differences to electricity using a two-capacitor circuit consisting of a $BaTiO_3$ ferroelectric capacitor and a regular capacitor. The model is based on the accurate free energy of Wang *et al.* [6] together with a circuit model that clarifies the thermodynamics behind this method of energy conversion. Our discussion of high-efficiency thermodynamic cycles for future devices leads us to introduce a "supercritical ferroelectric Carnot cycle," using the two-capacitor circuit as a building block.

The two main sources of loss identified and quantified in this paper are hysteresis of the phase transformation and leakage. Fortunately, there is a systematic materials-development procedure for reducing hysteresis in first-order phase transformations [30–36] that has recently been shown to be effective in oxides [37,38]. It remains to be seen whether this procedure is applicable to ferroelectric oxides. Reduction of leakage requires high-quality single-crystal films with attention paid to the design and quality of interfaces. Both of these sources of loss can be significantly improved in suitably doped $BaTiO_3$, as will be shown in forthcoming work.

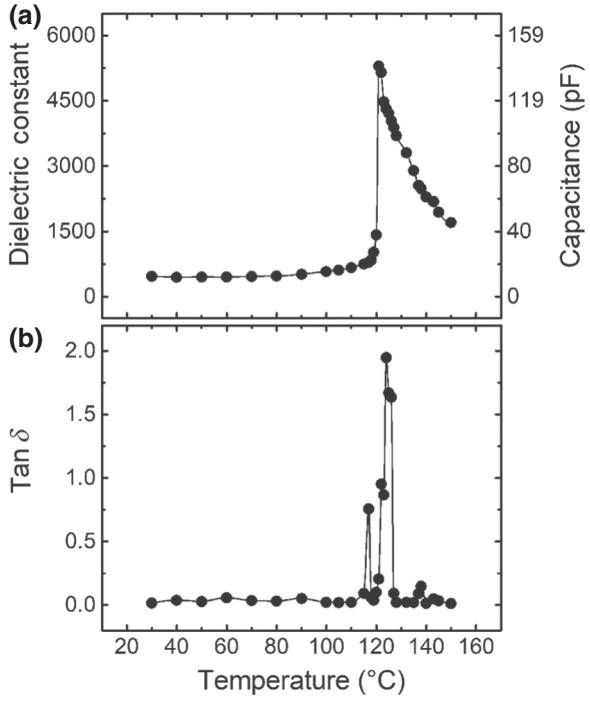

FIG. 1. The dielectric constant and capacitance (pF) (a) and loss tangent (b) of the $BaTiO_3$ single crystal as a function of temperature.

II. EXPERIMENTAL SECTION

The $BaTiO_3$ used for all measurements is provided by MTI Corporation. The material is 0.5-mm-thick (100) single crystal in the cubic paraelectric phase and contains both *a* and *c* domains in the tetragonal ferroelectric phase. The material provided by MTI measures 5 mm × 5 mm and is then cut into four quarters. The active ferroelectric capacitor area, A_f, used for these measurements is 1.5 mm^2. A Keithley 2220-30-1 dual-channel power supply is used to charge the circuit and a Keithley 2400 source meter is used for all voltage and current measurements. The temperature is monitored and controlled using a PLATINUM Series Omega CS8DPT universal bench-top digital controller. The ferroelectric capacitor is placed on top of a custom copper stage that consists of two 1/4-in. holes for the two 1/4-in.-diameter by 1-in.-long 80-W 120-V cartridge heaters (Tempco part no. 3618K421). All temperature measurements are taken using a thermocouple placed on the copper stage, directly next to the capacitor. The transformation temperature of the ferroelectric capacitor is measured as approximately 120°C using the PLATINUM Series Omega controller and a Keysight E4990A impedance analyzer; dielectric constant measurements are taken at 100 kHz with a 50 mV peak oscillating frequency.

III. ENERGY-CONVERSION DEMONSTRATION

A. Concept

To demonstrate solid-state energy conversion of small temperature differences to electricity using first-order phase transformations, we use the two-capacitor arrangement with an active $BaTiO_3$ ferroelectric capacitor connected in parallel to an ordinary capacitor, as shown in Fig. 2. An electrical load is represented by a resistor, *R*. The areas of the ferroelectric capacitor and of the ordinary capacitor plates are A_f and A_o, the thickness of the active ferroelectric capacitor is *d*, and the capacitance of the ordinary capacitor is C_o.

The outline of the energy-conversion procedure is as follows:

(1) Heat the ferroelectric capacitor to T^+.
(2) Charge the circuit to V_0 using an external battery.
(3) Remove the external battery from the circuit.
(4) Cool the ferroelectric capacitor to T^-.
(5) Heat the ferroelectric capacitor to T^+.
(6) Repeat steps 4 and 5.

During step 2, some amount of total charge, $Q_{\text{tot}} = Q_f + Q_o$, is introduced to the circuit and this charge distributes between the ferroelectric capacitor (Q_f) and the ordinary capacitor (Q_o) according to their capacitances. After step 3, the total charge, Q_{tot}, is trapped in the upper portion of the circuit. When the ferroelectric capacitor is cooled below the Curie temperature to T^-, the active material undergoes a phase transformation from the paraelectric phase to the ferroelectric phase and the polarization jumps up. This increase in polarization attracts charge from the ordinary capacitor, causing a current flow across the load and a redistribution of the total charge. When the ferroelectric capacitor is heated back above the Curie temperature to T^+, the polarization decreases, sending a current flow across the load in the opposite direction and another redistribution of the total charge. The key point is that $T^- < T^+$ arises from the differing electric fields in the capacitor, which bias the transformation temperature due to the effect of field on transformation temperature as mentioned in the introduction: this effect is embodied in the Clausius-Clapeyron equation and is a consequence of minimization of the free energy $\varphi(P,T) - EP$ of the ferroelectric subject to an electric field *E*. Thus, by fluctuating about the Curie temperature, a current is produced back and forth across the load.

1. Characterization of the ferroelectric and stability

For the free energy of the ferroelectric capacitor, we use the eighth-order model of Wang *et al.* [6] for $BaTiO_3$. In the full vectorial case, this is the following model:

$$\begin{aligned}\varphi(\mathbf{P},T) = {} & \alpha_1(T)(P_1^2+P_2^2+P_3^2)\\ & + \alpha_{11}(T)(P_1^4+P_2^4+P_3^4)\\ & + \alpha_{12}(T)(P_1^2P_2^2+P_2^2P_3^2+P_1^2P_3^2)\\ & + \alpha_{111}(T)(P_1^6+P_2^6+P_3^6)\\ & + \alpha_{112}[P_1^2(P_2^4+P_3^4)+P_2^2(P_1^4+P_3^4)\end{aligned}$$

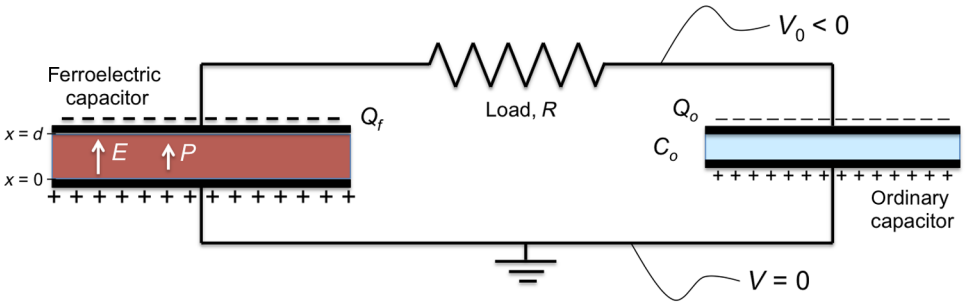

FIG. 2. A schematic of the solid-state energy-conversion demonstration circuit.

$$
\begin{aligned}
&+ P_3^2(P_1^4 + P_2^4)] \\
&+ \alpha_{123}(P_1^2 P_2^2 P_3^2) \\
&+ \alpha_{1111}(P_1^8 + P_2^8 + P_3^8) \\
&+ \alpha_{1112}[P_1^6(P_2^2 + P_3^2) + P_2^6(P_1^2 + P_3^2) \\
&+ P_3^6(P_1^2 + P_2^2)] \\
&+ \alpha_{1122}(P_1^4 P_2^4 + P_2^4 P_3^4 + P_1^4 P_3^4)) \\
&+ \alpha_{1123}(P_1^4 P_2^2 P_3^2 + P_1^2 P_2^4 P_3^2 + P_1^2 P_2^2 P_3^4), \quad (1)
\end{aligned}
$$

where (P_1, P_2, P_3) are components in the $\langle 100 \rangle$ directions. The units of polarization are $\mathrm{C/m^2}$ and T is in K, so that, for example, $\alpha_1(T)$ has units of V m/C, so that φ is in $\mathrm{V\,C/m^3 = J/m^3}$. The coefficients are given by the following:

$$
\begin{aligned}
&\alpha_1(T) = 3.61 \times 10^5 (T - 391), \quad \alpha_{112} = -2.2 \times 10^9, \\
&\alpha_{11}(T) = -1.83 \times 10^9 + 4. \times 10^6 T, \quad \alpha_{123} = 5.51 \times 10^{10}, \\
&\alpha_{12}(T) = -2.24 \times 10^9 + 6.7 \times 10^6 T, \quad \alpha_{1111} = 4.84 \times 10^{10}, \\
&\alpha_{111}(T) = 1.39 \times 10^{10} - 3.2 \times 10^7 T, \quad \alpha_{1112} = 2.53 \times 10^{11}, \\
&\alpha_{1122} = 2.8 \times 10^{11}, \quad \alpha_{1123} = 9.35 \times 10^{10},
\end{aligned}
$$

with suitable units consistent with the above.

Figure 3 shows a plot of the free energy vs polarization P_1 for various temperatures in the case that $P_2 = P_3 = 0$. For this model, the transition temperature is $T_c = 391$ K. Specialized to the case $P_2 = P_3 = 0$, the eighth-order model is as follows:

$$
\begin{aligned}
\varphi(P, T) &= \alpha_1(T)P^2 + \alpha_{11}(T)P^4 \\
&\quad + \alpha_{111}(T)P^6 + \alpha_{1111}P^8, \quad P = P_1.
\end{aligned}
$$

To find stable polarizations in a capacitor charged to voltage ΔV, we solve the problem

$$
\min_P \left[\varphi(P, T) - (\Delta V/d)P\right]. \quad (2)
$$

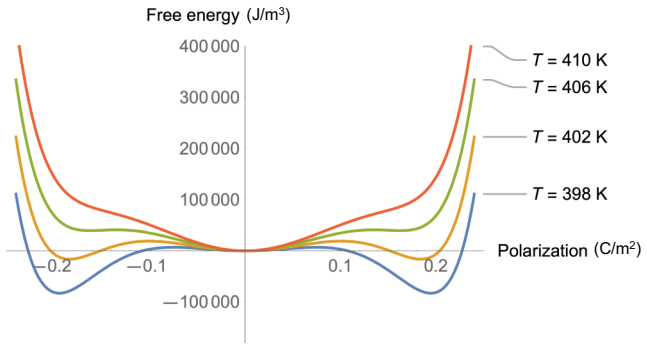

FIG. 3. A plot of the free energy given in Eq. (1) for a [100] polarization at various temperatures, showing the evolution of the energy wells with temperature.

We note that this problem is simplified: the exact energy is the sum of the energies of the ferroelectric and ordinary capacitors. For a justification of the simple expression given in Eq. (2), see the Appendix. The minimizing polarization $P = P(E, T)$, $E = \Delta V/d$, for the energy given in Eq. (2), is shown in Fig. 4. As expected, an applied field favors the ferroelectric phase and increases the transformation temperature. Note that according to this model, the jump in polarization also decreases as the temperature is raised, largely because of a strongly nonlinear response of both phases at the higher temperatures (see the curve labeled $T = 415$ K in Fig. 4). Of course, the model does not describe hysteresis.

The change of transformation temperature with electric field as shown in Fig. 4 is described by a Clausius-Clapeyron equation, thereby highlighting the role of latent heat. This is done by noticing that at each electric field $E = V/d > 0$, there is a temperature $T = T_c(E)$, depending on E, and two polarizations $P_p(E) < P_f(E)$ ("p" denotes paraelectric; "f" denotes ferroelectric) that equiminimize the total energy:

$$
\begin{aligned}
&\varphi[P_p(E), T_c(E)] - E\,P_p(E) \\
&\quad = \varphi[P_f(E), T_c(E)] - E\,P_f(E) \\
&\quad \le \varphi[P, T_c(E)] - E\,P, \quad (3)
\end{aligned}
$$

for all P. Therefore we have the necessary conditions,

$$
E = \frac{\partial \varphi}{\partial P}[P_p(E), T_c(E)] = \frac{\partial \varphi}{\partial P}[P_f(E), T_c(E)], \quad (4)
$$

(also evident in Fig. 4). We differentiate the equality in Eq. (3) with respect to T and use Eq. (4): some terms cancel and the remaining give the following:

$$
\begin{aligned}
&\left\{\frac{\partial \varphi}{\partial T}[P_p(E), T_c(E)] - \frac{\partial \varphi}{\partial T}[P_f(E), T_c(E)]\right\} T_c'(E) \\
&\quad = P_p(E) - P_f(E). \quad (5)
\end{aligned}
$$

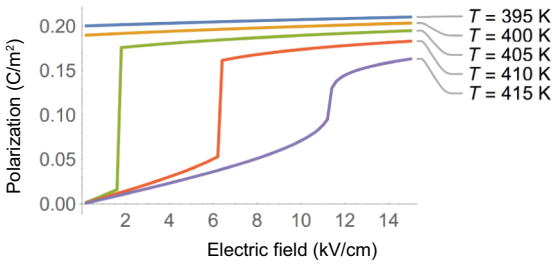

FIG. 4. A plot of the minimizing polarization vs the electric field at various temperatures according to the model of Wang *et al.* [6]. This is calculated by doing a numerical minimization of Eq. (2) for a grid of parameters E, T and then fitting the resulting function $P(E, T)$.

We introduce the entropies of the two phases,

$$S_f = -\frac{\partial \varphi}{\partial T}[P_f(E), T_c(E)], \tag{6}$$

and, from the Second Law of Thermodynamics in its simplest form, the *latent heat* $L = L(E)$ by

$$L = (S_p - S_f)T_c. \tag{7}$$

Substituting Eqs. (6) and (7) into Eq. (5), we obtain

$$T_c'(E) = T_c \frac{P_f(E) - P_p(E)}{L}, \tag{8}$$

the *Clausius-Clapeyron equation*, which links electric and thermal quantities. Note that, from this derivation, the Clausius-Clapeyron equation is still obtained if there is hysteresis, as long as the width of the hysteresis loop is independent of temperature and the line of equality of free energies (the "Maxwell line") is centered in the loop. These conditions are typically satisfied to good approximation in phase transformations with hysteresis, that is, to cases in which the initial paraelectric state is restored after one cycle, but there is hysteresis during the cycle. Typically, the more symmetric paraelectric phase has higher entropy and, since $P_f > P_p$, we have $T'(E) > 0$ and, as observed in Fig. 4, an electric field increases the transformation temperature. Also, $L > 0$, which means that during the transformation from the paraelectric to the ferroelectric phase, the material releases latent heat. Note that a small latent heat favors a big change of transformation temperature with the electric field.

B. Characterization of the circuit response

At step 1 of the energy-conversion procedure introduced in Sec. II A, the ferroelectric capacitor is heated to $T = T^+$. T^+ is chosen to be high enough so that, at the electric field $E = -V_0/d$, the active material is in the paraelectric phase, i.e., $T^+ > T_c(E)$. $T_c(E)$ can be calculated from the polarization of the ferroelectric (P_f) and paraelectric (P_p) phases at a given E using the Clausius-Clapeyron relationship given in Eq. (8).

During steps 2 and 3, a total charge Q_{tot} is supplied to the circuit by bringing the upper part of the circuit to a voltage V_0. Since, by definition, $\Delta V = V(-\infty) - V(\infty) = -V_0$, it is helpful to assume that $V_0 < 0$. Then, $E = -V_0/d > 0$, the polarization in the ferroelectric capacitor is positive, and the upper plates of both capacitors are negatively charged. At step 4, the ferroelectric capacitor is cooled from T^+ to T^-, beginning at $t = 0$. T^- is chosen to be low enough so that, at the electric field $E = -V_0/d$, the active material is in the ferroelectric phase, i.e., $T^- < T_c(E)$. Let us assume a time-dependent temperature

$$T(t), \quad T(0) = T^+, \quad T(\tau_c) = T^-, \tag{9}$$

with τ_c being the duration of the cooling. As discussed above, the charge is distributed between the two capacitors where the distribution depends on $T(t)$, but in all cases we have the following:

$$Q_{\text{tot}}(t) = Q_f(t) + Q_o(t) \tag{10}$$

and

$$Q_f(t) = -A_f P[E(t), T(t)], \quad Q_o(t) = C_o V(t). \tag{11}$$

We note that the first expression in Eq. (11) corresponds to complete screening. Using $E(t) = -V(t)/d$, the relationship between the voltage and the total charge is as follows:

$$Q_{\text{tot}}(t) = Q_f(t) + Q_o(t) = -A_f P[-V(t)/d, T(t)] + C_o V(t), \tag{12}$$

where $V(0) = V_0$.

At some time during cooling, the active material undergoes a phase transformation from the paraelectric phase to the ferroelectric phase and the polarization P jumps up. At this time, the total charge within the circuit Q_{tot} will need to be redistributed so that the ferroelectric capacitor holds more charge. In other words, the ordinary capacitor discharges onto the active ferroelectric capacitor through the load, creating a current flow $i(t)$. During this flow, Q_f becomes more negative, while Q_o increases, i.e., becomes less negative. Let $V_f(t)$ be the voltage on the left side of the resistor and $V_o(t)$ be the voltage on the right side. We can solve for $Q_f(t)$ using the following:

$$Q_f(t) = Q_f(0) - \int_0^{\tau_c} i(t)dt, \quad Q_o(t) = Q_o(0) + \int_0^{\tau_c} i(t)dt, \tag{13}$$

Equations (10)–(12), and Ohm's law:

$$V_o(t) - V_f(t) = i(t)R, \quad V_f(0) = V_o(0) = V_0. \tag{14}$$

With these relations, all equations are satisfied except the first of Eqs. (11), which remains as the implicit differential equation,

$$Q_f(t) = -A_f P\left[\frac{Q_f(t) - Q_{\text{tot}}}{d\, C_o} - \frac{R}{d}\dot{Q}_f(t), T(t)\right]. \tag{15}$$

Inverting $E = \partial\varphi(P,T)/\partial P$, where φ is the free energy and restricting to the stable branches of the free energy,

i.e., $E = \partial\varphi(P,T)/\partial P|_{\text{stable}}$, gives

$$\dot{Q}_f(t) = \frac{Q_f(t) - Q_{\text{tot}}}{R\,C_o} - \left(\frac{d}{R}\right)\left.\frac{\partial\varphi[-Q_f(t)/A_f, T(t)]}{\partial P}\right|_{\text{stable}}, \tag{16}$$

subject to an initial condition for $Q_f(0)$ that comes from step 1. Note that this equation is satisfied if we use $T(t) = T^+$ and $Q_f = Q_f(0) = Q_{\text{tot}} - Q_o(0)$.

Essentially, Eq. (16) is a dissipative differential equation the solution of which passes from one equilibrium state at T^+ to another at T^-, so it is first worth looking at the equilibrium states E^+, P^+ and E^-, P^-. (We use the superscript notation $\pm$ to denote these equilibrium states corresponding to $T^\pm$.) At equilibrium, we have the following:

$$T = T^+: \quad Q_f^+ = -A_f P(-V^+/d, T^+), \quad Q_o^+ = C_o V^+,$$
$$T = T^-: \quad Q_f^- = -A_f P(-V^-/d, T^-), \quad Q_o^- = C_o V^-,$$

and at all times, we satisfy Eq. (10). We can represent these equations graphically. By eliminating $Q_o^\pm$ from Eq. (10) and substituting $E^\pm$ for $-V^\pm/d$, we have the following:

$$P(E^-, T^-) - P(E^+, T^+) = \frac{1}{A_f}(Q_f^+ - Q_f^-) = \frac{C_o d}{A_f}(E^+ - E^-). \tag{17}$$

Equation (17) tells us that maximizing the charge transfer is equivalent to maximizing the difference in polarization. Eliminating $Q_f^\pm$ and rearranging, we have the following:

$$\frac{P(E^+, T^+) - P(E^-, T^-)}{E^+ - E^-} = -\frac{C_o d}{A_f}. \tag{18}$$

Equation (18) says that the slope of the line connecting the two equilibrium states, dP/dE, is equal to minus the reference capacitance C_o times the purely geometric aspect ratio d/A_f of the active ferroelectric capacitor. This is illustrated in Fig. 5. This graphical description tells us that the relationship between the equilibrium states can be controlled via either the geometry of the ferroelectric capacitor or the capacitance of the ordinary capacitor.

We note that when E^- is very small, the field on the ferroelectric capacitor may not be sufficient to transform the ferroelectric capacitor to the poled ferroelectric phase, as predicted by the above energy minimization. As seen from the polarization values recorded in Fig. 6, our fields are sufficient for nearly complete transformation and poling as predicted by the model.

IV. COMPARISON BETWEEN THEORY AND EXPERIMENT

The circuit in Fig. 2 is constructed using a (100) $BaTiO_3$ single crystal with a thickness of 0.5 mm and an area of 1.5 mm^2, purchased from MTI, a 5.1 kΩ resistor, and reference capacitors with capacitances of $C_o = 1$ pF, 1 μF, and 10 μF. The circuit is charged to $V_0 = 60$ V using a dc voltage supply at $T^+ = 124\,^\circ$C and then the voltage supply is removed at $t = 0$. The temperature of the ferroelectric capacitor is then fluctuated between $T^+ = 124\,^\circ$C and $T^- = 114\,^\circ$C. A low-temperature fluctuation frequency (approximately 0.01 Hz) is used for this first demonstration; the effect of frequency will be the subject of a future experiment. The electric field across the ferroelectric capacitor is monitored by measuring the voltage across the ferroelectric capacitor $V_f(t)$ and using $E_f(t) = -V_f(t)/d$. The polarization across the ferroelectric capacitor is monitored using a Sawyer-Tower bridge [39] consisting of an additional 1-μF capacitor C_{ST} in series with the ferroelectric capacitor and using $P(t) = C_{\text{ST}}V_{\text{ST}}(t)/A_f$, where V_{ST} is the voltage across the Sawyer-Tower capacitor. Finally, the current $i(t)$ flowing between the two capacitors is measured in series with the resistor.

The results in Fig. 6 show the circuit response for the $C_o = 1$ μF case. Figure 6 shows both the measured experimental data as well as the predicted behavior calculated using the free-energy model and the relations discussed throughout Sec. III. As the material transforms between the paraelectric and ferroelectric phases, the electric field and the polarization can be seen jumping between the two equilibrium states at T^+ and T^-, as illustrated in Fig. 5. Each time the polarization jumps, the total charge is redistributed between the ferroelectric and ordinary capacitors and current flows through the resistor. This current is directly related to the power $[i(t)^2R]$ being dissipated through the resistor.

As shown in Fig. 5, the slope of the line connecting the two equilibrium states on a polarization vs electric field plot can be calculated using the capacitance of the ordinary capacitor and the geometric aspect ratio of the ferroelectric capacitor (Eq. 18). This relation is verified using

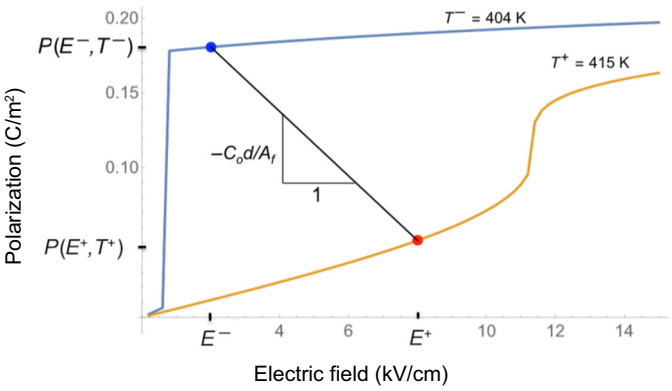

FIG. 5. A graphical construction for the description of the equilibrium states at temperatures T^+ and T^-. The choices $T^- = 404$ K and $T^+ = 415$ K are just for the purpose of illustration.

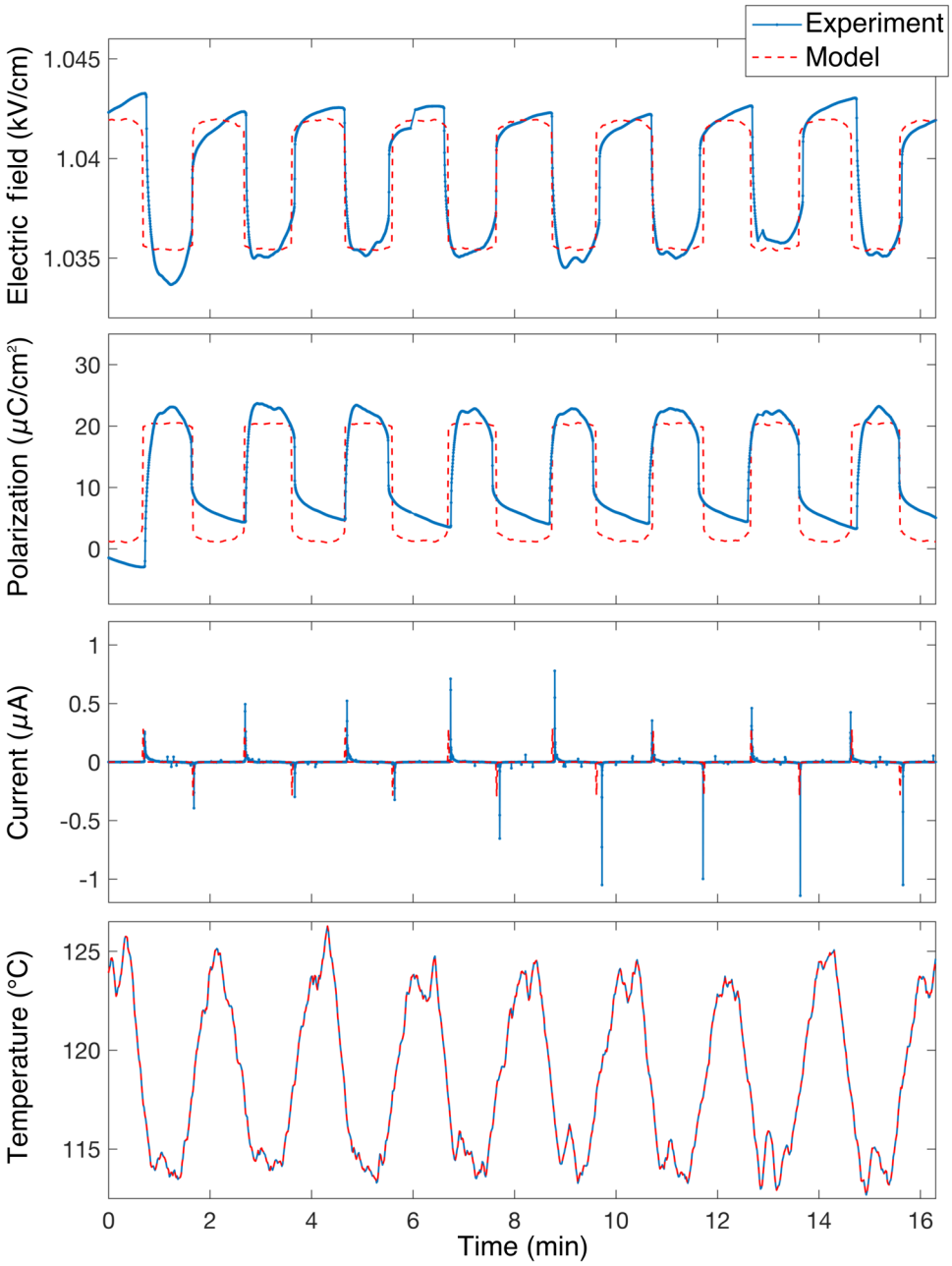

FIG. 6. The direct conversion of small temperature fluctuations to electricity using first-order phase transformations in a ferroelectric capacitor.

three different ordinary reference capacitors C_o. Table I shows the experimentally measured slope, dP/dE, and the theoretical slope calculated using $dP/dE = -C_o d/A$. The results show very close agreement between the experimental and theoretical values. Note that the experimentally measured slope for the $C_o = 1$ pF case appears to be several orders of magnitude smaller than the calculated theoretical slope, but in actuality the line is approximately horizontal and so both slopes are approximately zero.

It should be noted that the ferroelectric capacitor shows signs of charge leakage that result in gradual changes in $V_f(t)$ and $V_{ST}(t)$. In Fig. 6, these leakage effects are fitted and subtracted to focus on the validation of the energy-conversion demonstration. The leakage does not affect the current measurements. As mentioned in Sec. I, reduction of leakage requires high-quality single-crystal films with attention paid to the design and quality of interfaces.

V. THERMODYNAMIC CYCLES

Looking ahead, it will be necessary to examine and optimize the energy densities, power densities, and thermodynamic efficiencies of the conversion of waste heat

TABLE I. The experimental vs the theoretical dP/dE.

Reference capacitance, C_o	ExperimentalP dP/dE (C/Vm)	Theoretical $dP/dE = -C_o d/A$ (C/Vm)
1 pF	9.41×10^{-14}	2.66×10^{-10}
1 μF	2.58×10^{-4}	2.66×10^{-4}
10 μF	2.66×10^{-3}	2.66×10^{-3}

to electricity using first-order phase transformations in ferroelectrics. Historically, Ericsson cycles—or Olsen cycles, as they are known in the pyroelectric literature—have been used in energy-conversion technologies containing pyroelectric and relaxor ferroelectric materials [5,20–22,25,26]. However, these cycles do not take advantage of the large mixed-phase region in first-order ferroelectric phase transformations or the sharp jumps in polarization. Due to the similarities between first-order phase transformations in ferroelectrics and first-order phase transformations in steam, it is natural to take inspiration from steam cycles for ferroelectric energy conversion.

Analogous to the ideal Carnot vapor cycle, the ideal ferroelectric Carnot cycle is composed of four reversible processes:

1–2: Adiabatic charging
2–3: Isothermal depolarization
3–4: Adiabatic discharging
4–1: Isothermal polarization

Step 1–2 is the adiabatic charging of a ferroelectric-paraelectric mixture to a saturated ferroelectric (analogous to the adiabatic compression of a liquid-vapor mixture to saturated liquid). Step 2–3 is the isothermal phase transformation from the ferroelectric phase to the paraelectric phase (analogous to the isothermal vaporization from saturated liquid to saturated vapor). Step 3–4 is the adiabatic discharging of the saturated ferroelectric phase into the two-phase ferroelectric-paraelectric mixture region (analogous to the adiabatic expansion of saturated vapor). Step 4–1 is the isothermal partial phase transformation of the ferroelectric-paraelectric mixture toward the ferroelectric phase (analogous to the partial condensation of the liquid-vapor mixture). The process curves associated with the ideal ferroelectric Carnot cycle are shown in red in the temperature vs entropy, $T-S$, and polarization vs electric field, $P-E$, diagrams in Figs. 7(a) and 7(b).

The ideal ferroelectric Carnot cycle will have the highest thermal efficiency of any possible cycle for a given temperature difference $\Delta T = T^+ - T^-$:

$$\eta_{\text{th,Carnot}} = \frac{W_{\text{net}}}{Q_{\text{in}}} = 1 - \frac{T^-}{T^+}, \tag{19}$$

where the net work W_{net} is equal to the area enclosed by the process curves. As with the ideal Carnot vapor cycle, the efficiency of the ideal ferroelectric Carnot cycle will be reduced by any irreversible processes. However, in the ferroelectric Carnot cycle case, a device that operates with near-perfect reversibility is conceivable by using highly reversible phase transformations. Furthermore, there is a systematic materials-development procedure for maximizing reversibility in first-order phase transformations in shape-memory alloys [30–34,36] and strong ferromagnetic phase transformations [35], which has recently shown to be effective in oxides [37,38]. It is an open question whether this procedure can be used to engineer ferroelectrics for high reversibility.

Because of the small temperature difference, the ideal Carnot efficiency for the red cycle shown in Figs. 7(a) and 7(b) is 0.7%. Of course, for applications where there is an overabundance of waste heat, the efficiency of a device may be of much less concern than the energy density. The energy density of an ideal ferroelectric Carnot cycle is limited by the size of the mixed-phase region. For example, the red cycle in Figs. 7(a) and 7(b) would produce an energy density of 0.065 J/cm^3. Another way of achieving an ideal Carnot cycle that maximizes both efficiency and energy density is shown in blue in Figs. 7(a) and 7(b). This version of the ferroelectric Carnot cycle is analogous to a supercritical Carnot vapor cycle and so we call it a "supercritical ferroelectric Carnot cycle." By extending the cycle above the mixed-phase region, this supercritical Carnot cycle produces an energy density of 0.49 J/cm^3 and a thermal efficiency of 7%. These are very reasonable values considering that the operative temperature difference is only 30°C. If T^+ is increased so that $\Delta T = 70\,^\circ$C, then the energy density increases to 1.15 J/cm^3 with a thermal efficiency of 15%. For comparison, the highest values for energy density and efficiency ever reported for a pyroelectric waste heat to electricity converter using a ΔT of 70°C are 1.06 J/cm^3 and 3.6% [5].

In addition to designing a ferroelectric with near-perfect reversibility, the main challenge of the ferroelectric Carnot cycle will be to maintain constant polarization during adiabatic charging and discharging (steps 4–1 and 2–3). However, the ferroelectric–ordinary-capacitor construction shown in Fig. 2 and our understanding of the relationship between equilibrium states (Eq. 18) can be employed here. Our proposed procedure for achieving a supercritical ferroelectric Carnot cycle is as follows.

0: Charge the circuit to V_1 at T^-.
1–2: Open the switch and increase the temperature to T^+. (E_f will increase from $E_{f,1}$ to $E_{f,2}$.)
2–3: Close the switch and decrease the voltage from $V_2 = E_{f,2}/d$ to V_3.
3–4: Open the switch and decrease the temperature to T^-. (E_f will decrease from $E_{f,3}$ to $E_{f,4}$.)

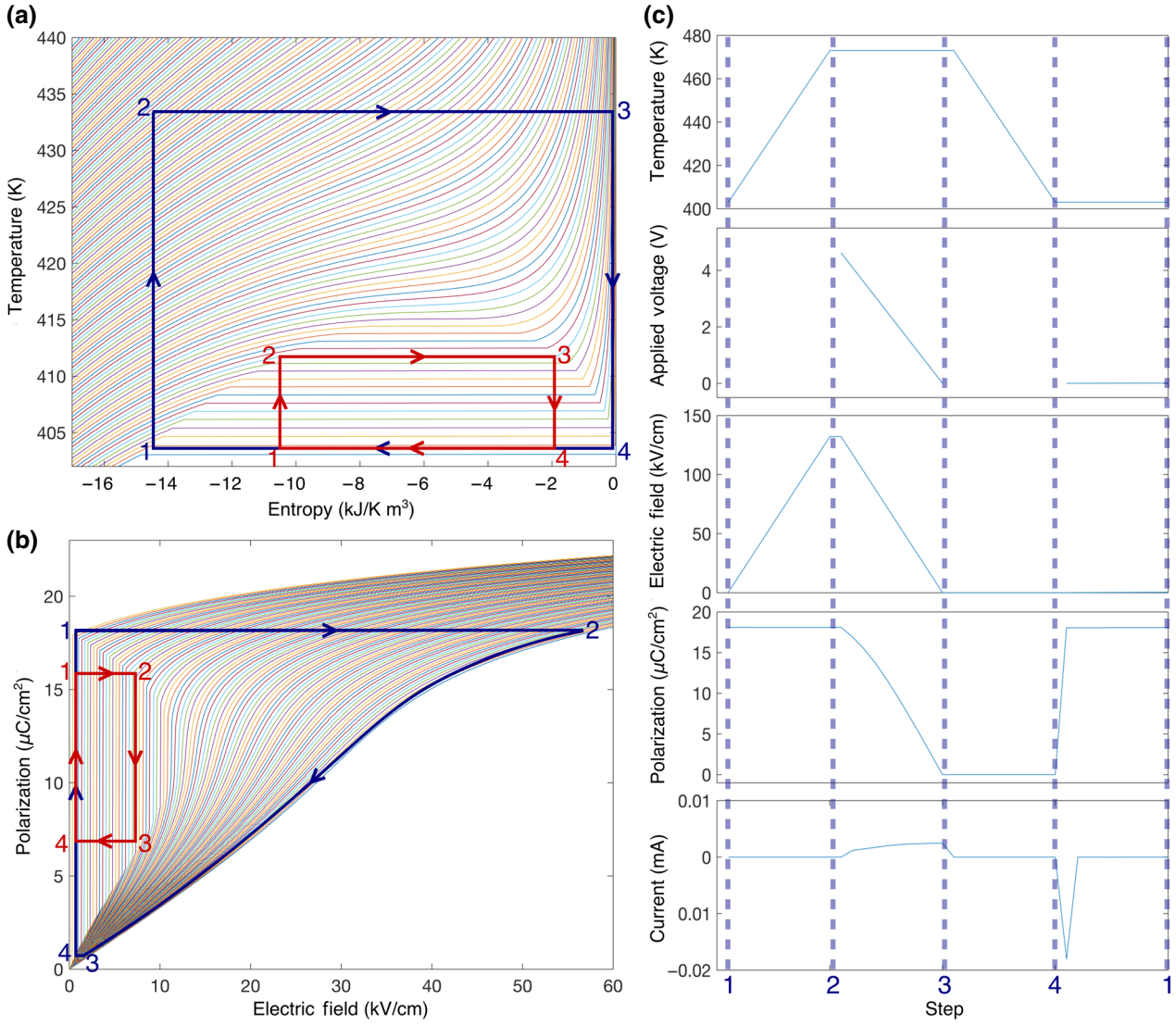

FIG. 7. Example $T-S$ (a) and $P-E$ (b) process curves for an ideal ferroelectric Carnot cycle (in red) and a supercritical ferroelectric Carnot cycle (in blue): (a) lines of constant electric field; (b) lines of constant temperature. The inputs and circuit response for the supercritical ferroelectric Carnot cycle are shown in (c).

4–1: Close the switch and increase the voltage from $V_3 = E_{f,3}/d$ to $V_4 = V_1$.

This procedure requires an initiation step (step 0) and the rest of the procedure can be repeated cyclically. As shown in Fig. 5, when the switch is open and the circuit alternates between two temperatures, the ferroelectric capacitor will alternate between two equilibrium states, $P(E^+,T^+),E^+$ and $P(E^-,T^-),E^-$. The slope of the line connecting the equilibrium states is equal to $-C_o d/A_f$ as given in Eq. (18). By using a reference capacitor with a very low capacitance, it is possible to increase or decrease the temperature without changing the polarization (see the $C_o = 1$ pF case in Table I). Note that this can also be achieved by increasing A_f and/or decreasing d. Following Eqs. (1) and (6), the only change in entropy in a constant-polarization process will be from the change in temperature.

The supercritical ferroelectric Carnot cycle procedure described above is simulated in Fig. 7(c) using the equations from Sec. III and the values listed in Table II. The inputs (temperature and applied voltage) and outputs [$E_f(t)$, $P_f(t)$, and $i(t)$] are shown as a function of the process step. This cycle would produce an energy density of 1.15 J/cm^3 and a thermal efficiency of 15% (larger than that of [5] with the same ΔT and requiring less than half the electric field). As with any thermodynamic cycle, the performance metrics will improve with temperature

TABLE II. Values of parameters used in the supercritical ferroelectric Carnot cycle calculations.

Parameter	Description	Value	Unit
d	Thickness of ferroelectric capacitor	350	μm
A_f	Area of ferroelectric capacitor	10×10	mm^2
C_o	Capacitance of ordinary capacitor	0.1	pF
T^-	Minimum temperature	403.5	K
T^+	Maximum temperature	473.5	K
V_1	Applied voltage at point 1	-15.7	V
V_3	Applied voltage at point 3	-53.0	V

difference, but the temperature difference will be limited in practice. In Fig. 6(a), the lines are lines of constant electric field, where higher-temperature (supercritical) transitions require higher and higher electric fields. Thus, the high-temperature processes will likely be limited by the breakdown voltage of the film.

VI. CONCLUSION

In this paper, the direct conversion of heat to electricity is demonstrated using first-order phase transformations in lead-free ferroelectrics. This simple demonstration illustrates how the growing abundance of energy stored on earth at small temperature difference can be converted to useful electrical power. The major contributions of this paper are summarized below.

(1) The thermodynamics of solid-state energy conversion using first-order phase transformations in $BaTiO_3$ are examined using a free-energy approach. Using this approach, we derive the well-known Clausius-Clapeyron relation between the transformation temperature and the electric field and discuss the importance of the Clausius-Clapeyron relation in splitting the transformation temperature and opening up the mixed-phase region.

(2) A simple two-capacitor circuit consisting of an active $BaTiO_3$ capacitor, an ordinary capacitor, and a load represented by a resistor is introduced to demonstrate the direct conversion of heat to electricity. The circuit response is characterized using the free-energy model of the active $BaTiO_3$. The relationship between equilibrium states is found to be dependent on the capacitance of the ordinary capacitor and the geometric aspect ratio of the active ferroelectric capacitor.

(3) The energy-conversion demonstration device is tested experimentally. By fluctuating the temperature on the active $BaTiO_3$ capacitor by $\pm 5^\circ$C about 119 °C, the paraelectric-to-ferroelectric phase transformation inside the active $BaTiO_3$ capacitor causes a current flow across the resistor, dissipating power. The predicted circuit response is validated by experimental measurements of the polarization, the electric field, and the current flow.

(4) A supercritical ferroelectric Carnot cycle that would maximize thermodynamic efficiency and work output for a given temperature difference is introduced. The practical implementation of this cycle consists of using the two-capacitor circuit to adiabatically charge and discharge in addition to reversible underlying phase transformations. Using a temperature difference of 70 °C, this cycle would produce an energy density of 1.15 J/cm^3 and a thermal efficiency of 15% (larger than that of the most successful pyroelectric energy-conversion demonstration [5] with the same ΔT and requiring less than half the electric field). Due to the importance of reversibility, the supercritical ferroelectric Carnot cycle would greatly benefit from a highly reversible paraelectric-to-ferroelectric phase transformation that has been demonstrated in shape-memory alloys [30–34,36], ferromagnetic materials [35], and, more recently, in oxides [37,38].

ACKNOWLEDGMENTS

The authors thank the reviewers for helpful comments. A.B. was supported by a UMN President's Postdoctoral Fellowship and W.N. received partial support from the Norwegian Centennial Chair Program (NOCC). All authors received support from the Institute on the Environment (RDF fund). R.D.J. also benefited from the support of the National Science Foundation (NSF) (DMREF-1629026), the Office of Naval Research (ONR) (N00014-18-1-2766), the Multidisciplinary University Research Initiative (MURI) (FA9550-18-1-0095), the Medtronic Corporation, and a Vannevar Bush Faculty Fellowship. R.D.J. thanks the Isaac Newton Institute for Mathematical Sciences for support during the program "The mathematical design of new materials" by the EPSRC under Grant No. EP/R014604/1.

APPENDIX RELATION BETWEEN THE GENERAL EXPRESSION FOR THE ENERGY OF THE TWO-CAPACITOR SYSTEM AND THE SIMPLIFIED MODEL

In this Appendix, we give the derivation of the $P-E$ relation and a Clausius–Clapeyron-type equation from a general model that includes the energies of both the ferroelectric and ordinary capacitors in a closed system. This analysis justifies the simple model used in this paper.

1. Total free energy of the two-capacitor system

We consider the closed system consisting of the ferroelectric and ordinary capacitors. The total energy of the ferroelectric plus ordinary capacitors in J is as follows:

$$A_f\, d_f\, \varphi(P,T) + \tfrac{1}{2} C_o\, V^2, \tag{A1}$$

where V is the voltage across the ordinary capacitor, A_f is the area of the ferroelectric capacitor, and d_f is the distance between the plates of the ferroelectric capacitor. V is in volts and C_o is in farads. The given information is the value of the total charge $Q_{\rm tot} = Q_o + Q_f = C_o V - A_f P$, where P is the polarization of the ferroelectric capacitor. $Q_{\rm tot}$ is distributed between the ordinary and ferroelectric capacitors according to free-energy minimization, i.e., the minimization of Eq. (A1). Thus, P is a good independent variable and the general minimization problem is, given $Q_{\rm tot}$, as follows:

$$\min_P \left[A_f\, d_f\, \varphi(P,T) + \frac{1}{2} C_o \left(\frac{Q_{\rm tot} + A_f P}{C_o} \right)^2 \right] = \min_P \left[A_f\, d_f\, \varphi(P,T) + \frac{1}{2\, C_o} \left(Q_{\rm tot} + A_f P \right)^2 \right]. \quad \text{(A2)}$$

Expanding the last term, we can drop the constant $Q_{\rm tot}^2/2C_o$ term, since we are doing energy minimization. Then, simplifying, we have the following:

$$\min_P \left[A_f\, d_f\, \varphi(P,T) + \frac{1}{2\, C_o} \left(2 A_f\, Q_{\rm tot} P + A_f^2 P^2 \right) \right]. \quad \text{(A3)}$$

2. First variation

In the expression given in Eq. (A3), we have the independent variable P and otherwise only various fixed constants, such as $T = \text{const.}$ and $A_f, d_f, \ldots$. So, at a minimizer the first derivative is zero: this gives

$$A_f\, d_f \frac{\partial \varphi(P,T)}{\partial P} + \frac{1}{C_o} \left(A_f\, Q_{\rm tot} + A_f^2 P \right) = 0. \quad \text{(A4)}$$

Substituting $Q_{\rm tot} = C_o V - A_f P$, we have

$$A_f\, d_f \frac{\partial \varphi(P,T)}{\partial P} + \frac{1}{C_o} \left[A_f \left(C_o V - A_f P \right) + A_f^2 P \right] = 0, \quad \text{(A5)}$$

that is,

$$\frac{\partial \varphi(P,T)}{\partial P} = -\frac{V}{d_f} = E. \quad \text{(A6)}$$

So, the first variation gives the same condition as minimizing $\varphi - EP$ over P. Note that for the general problem, we should not think of E as a given constant and look for a solution P of Eq. (A6). That is because P and E are coupled by the condition $Q_{\rm tot} = C_o V - A_f P = -d_f C_o E - A_f P$. Thus, we expect that, in the case of multiple solutions of Eq. (A6), they will be of the form, say, (P_1, E_1), (P_2, E_2), etc., as is verified below.

3. Coexistence and a Clausius–Clapeyron-type equation

At high temperature, $\varphi(P,T)$ is convex in P, and also the term $1/2\, C_o \left(2 A_f\, Q_{\rm tot} P + A_f^2 P^2 \right)$ is strictly convex in P. Therefore, at high temperature the total energy is strictly convex and has a single minimizer corresponding to the paraelectric phase. As we lower the temperature, φ develops energy wells and we expect multiple solutions P_1, P_2 of the minimization problem Eq. (A3).

In the simplified problem, $\min_P(\varphi - EP)$ with E given, a well-known graphical interpretation of multiple solutions is that we fix T and push a line with slope E up against the graph of $\varphi(P,T)$. The common touching points are then solutions of the minimization problem. This is the case treated in this paper.

The general problem given in Eq. (A3) also has a geometric interpretation. Given $Q_{\rm tot}$, suppose that we have multiple minimizers $P_1, P_2, \ldots$ of the energy given in Eq. (A3). Then, for all P,

$$\begin{aligned} &A_f\, d_f\, \varphi(P,T) + \frac{1}{2\, C_o} \left(2 A_f\, Q_{\rm tot} P + A_f^2 P^2 \right) \\ &\quad \geq A_f\, d_f\, \varphi(P_1,T) + \frac{1}{2\, C_o} \left(2 A_f\, Q_{\rm tot} P_1 + A_f^2 P_1^2 \right) \\ &\quad = A_f\, d_f\, \varphi(P_2,T) + \frac{1}{2\, C_o} \left(2 A_f\, Q_{\rm tot} P_2 + A_f^2 P_2^2 \right) \\ &\quad = \text{etc.} \end{aligned} \quad \text{(A7)}$$

That is, rearranging,

$$\begin{aligned} \varphi(P,T) &\geq \varphi(P_1,T) + \frac{1}{2\, C_o d_f} \times \left[2 Q_{\rm tot} (P_1 - P) + A_f \left(P_1^2 - P^2 \right) \right] \\ &= \varphi(P_2,T) + \frac{1}{2\, C_o d_f} \times \left[2 Q_{\rm tot} (P_2 - P) + A_f \left(P_2^2 - P^2 \right) \right] \\ &= \text{etc.} \end{aligned} \quad \text{(A8)}$$

The right-hand sides of Eqs. (A8) describe exactly the same parabola due to the equality on the right-hand sides of Eqs. (A7). Thus, multiple solutions of the general problem correspond geometrically to pushing a parabola [given by either right-hand side of Eq. (A8)] up against the graph of $\varphi(P,T)$ and looking for touching points (see Fig. 9). Note that from Eq. (A8), the parabola is concave down.

In seeking a precise relation between the general problem and the simplified problem, we need to quantify how close the parabola is to a line and what dimensionless parameter governs the closeness. This is quantified by the following argument. Fix T. On the graph of $\varphi(P,T)$ in Fig. 9, suppose that we start at $[P_1, \varphi(P_1,T)]$ and move

TABLE III. Experimental vs theoretical values for the left-hand side of Eq. (A12).

Reference capacitance, C_o	Experimental	Theoretical
1 pF	1.7	1.7
1 μF	2.7×10^{-4}	3.4×10^{-4}
10 μF	2.7×10^{-5}	3.3×10^{-5}

on a straight line in the direction of the tangent through this point, as in the simplified problem. The parabola is nearly linear on the scale of Fig. 9 if, as we move along this tangent toward P_2, we arrive close to $[P_2, \varphi(P_2, T)]$, that is,

$$\varphi(P_1, T) + (P_2 - P_1)\frac{\partial \varphi(P_1, T)}{\partial P} \approx \varphi(P_2, T). \tag{A9}$$

We eliminate $\varphi(P_1, T) - \varphi(P_2, T)$ from Eq. (A9) using the equality on the right-hand side of Eq. (A7). Also, we use the first variation $\partial\varphi(P_1, T)/\partial P = E_1$ to eliminate $\partial\varphi(P_1, T)/\partial P$ from Eq. (A9). Finally, we substitute $Q_{\text{tot}} = -d_f C_o E_1 - A_f P_1$ in Eq. (A9). Then, Eq. (A9) becomes the following:

$$\frac{1}{2C_o d_f}\left[(-2d_f C_o E_1 - A_f P_1)(P_2 - P_1) + A_f (P_2^2 - P_1^2)\right] + (P_2 - P_1)E_1 \approx 0, \tag{A10}$$

that is,

$$\frac{A_f}{2C_o d_f}\left[P_2(P_2 - P_1)\right] \approx 0. \tag{A11}$$

Here, the left-hand side is in units of energy density, J/m^3 [cf. Eq. (A9)]. To make it dimensionless in a way that is meaningful for energy conversion using the method developed in this paper, we choose $P_2 = P_f$ as a typical polarization of the ferroelectric phase, $P_1 = 0$ corresponding to the paraelectric phase, and we divide by the typical

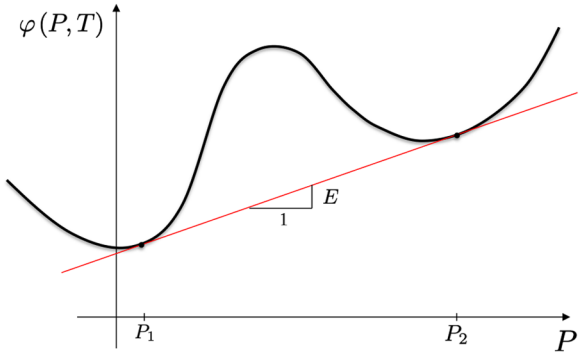

FIG. 8. The classic construction for the simplified problem.

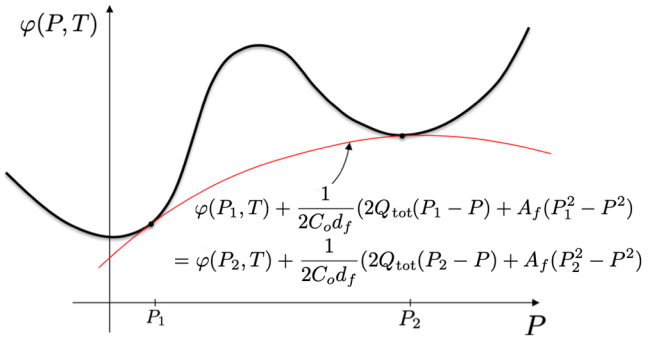

FIG. 9. The construction for the general problem.

maximum difference in energy density occurring during a cycle, $\Delta\mathcal{E}$. We arrive at the following dimensionless criterion:

$$\frac{A_f P_f^2}{2(\Delta\mathcal{E})d_f C_o} \ll 1. \tag{A12}$$

For the capacitors, geometry, and material data used in this paper, experimentally measured and theoretical values for this dimensionless number are shown in Table III.

The trend shows that the parabola shown in Fig. 9 is very close to the line given by the classical construction (Fig. 8). The simplified model is therefore justified under the conditions of the demonstration reported in the text.

[1] M. Kohl, *Shape Memory Microactuators, Microtechnology and MEMS* (Springer-Verlag, Berlin, Heidelberg, 2004).
[2] C. R. Bowen, J. Taylor, E. LeBoulbar, D. Zabek, A. Chauhan, and R. Vaish, Pyroelectric materials and devices for energy harvesting applications, Energy Environ. Sci. **7**, 3836 (2014).
[3] P. Muralt, Ferroelectric thin films for micro-sensors and actuators: A review, J. Micromech. Microeng. **10**, 136 (2000).
[4] S. Trolier-McKinstry and P. Muralt, Thin film piezoelectrics for MEMS, J. Electroceram. **12**, 7 (2004).
[5] S. Pandya, J. Wilbur, J. Kim, R. Gao, A. Dasgupta, C. Dames, and L. W. Martin, Pyroelectric energy conversion with large energy and power density in relaxor ferroelectric thin films, Nat. Mater. **17**, 432 (2018).
[6] Y. L. Wang, A. K. Tagantsev, D. Damjanovic, N. Setter, V. K. Yarmarkin, A. I. Sokolov, and I. A. Lukyanchuk, Landau thermodynamic potential for $BaTiO_3$, J. Appl. Phys. **101**, 104115 (2007).
[7] C. Zhang, Y. Song, M. Wegner, E. Quandt, and X. Chen, Power-Source-Free Analysis of Pyroelectric Energy Conversion, Phys. Rev. Appl. **12**, 014063 (2019).
[8] T. Takenaka and H. Nagata, Current status and prospects of lead-free piezoelectric ceramics, Elecroceram. IX **25**, 2693 (2005).
[9] E. Ringgaard and T. Wurlitzer, Lead-free piezoceramics based on alkali niobates, Elecroceram. IX **25**, 2701 (2005).

[10] R. G. Rhodes, Barium titanate twinning at low temperatures, Acta Crystallogr. **4**, 105 (1951).
[11] A. von Hippel, R. G. Breckenridge, F. G. Chesley, and L. Tisza, High dielectric constant ceramics, Ind. Eng. Chem. Res. **38**, 1097 (1946).
[12] C. F. Buhrer, Some properties of bismuth perovskites, J. Chem. Phys. **36**, 798 (1962). https://doi.org/10.1063/1.1732613.
[13] L. Curecheriu, S.-B. Balmus, M. T. Buscaglia, V. Buscaglia, A. Ianculescu, and L. Mitoseriu, Grain size-dependent properties of dense nanocrystalline barium titanate ceramics, J. Am. Ceram. Soc. **95**, 3912 (1998). https://onlinelibrary.wiley.com/doi/pdf/10.1111/j.1551-2916.2012.05409.x.
[14] T. Kanata, T. Yoshikawa, and K. Kubota, Grain-size effects on dielectric phase transition of $BaTiO_3$ ceramics, Solid State Commun. **62**, 765 (1987).
[15] Waste Heat Recovery, *Technology and Opportunities in the U.S. Industry*, Tech. Rep. (U.S. Department of Energy, 2008).
[16] Estimated U.S. Energy Consumption in 2016 (2017).
[17] V. Srivastava, Y. Song, K. Bhatti, and R. D. James, The direct conversion of heat to electricity using multiferroic alloys, Adv. Energy Mater. **1**, 97 (2011).
[18] Y. Song, C. Leighton, and R. D. James, in *Heusler Alloys* (Springer, 2016), p. 269–291.
[19] A. S. Mischenko, Q. Zhang, J. F. Scott, R. W. Whatmore, and N. D. Mathur, Giant electrocaloric effect in thin-film $PbZr_{0.95}Ti_{0.05}O_3$, Science **311**, 1270 (2006).
[20] R. B. Olsen, J. M. Briscoe, D. A. Bruno, and W. F. Butler, A pyroelectric energy converter which employs regeneration, Ferroelectrics **38**, 975 (1981).
[21] R. B. Olsen, D. A. Bruno, and J. M. Briscoe, Pyroelectric conversion cycles, J. Appl. Phys. **58**, 4709 (1985).
[22] F. Y. Lee, H. R. Jo, C. S. Lynch, and L. Pilon, Pyroelectric energy conversion using PLZT ceramics and the ferroelectric-ergodic relaxor phase transition, Smart Mater. Struct. **22**, 025038 (2013).
[23] G. Sebald, S. Pruvost, and D. Guyomar, Energy harvesting based on Ericsson pyroelectric cycles in a relaxor ferroelectric ceramic, Smart Mater. Struct. **17**, 015012 (2007).
[24] A. Khodayari, S. Pruvost, G. Sebald, D. Guyomar, and S. Mohammadi, Nonlinear pyroelectric energy harvesting from relaxor single crystals, IEEE Trans. Ultrason. Ferroelectr. Freq. Control **56**, 693 (2009).
[25] A. Navid, D. Vanderpool, A. Bah, and L. Pilon, Towards optimization of a pyroelectric energy converter for harvesting waste heat, Int. J. Heat Mass Transf. **53**, 4060 (2010).
[26] Ashcon Navid and Laurent Pilon, Pyroelectric energy harvesting using Olsen cycles in purified and porous poly(vinylidene fluoride-trifluoroethylene) [P(VDF-TrFE)] thin films, Smart Mater. Struct. **20**, 025012 (2011).
[27] A. Giguere, M. Foldeaki, B. R. Gopal, R. Chahine, T. K. Bose, A. Frydman, and J. A. Barclay, Direct Measurement of the "Giant" Adiabatic Temperature Change in $Gd_5Si_2Ge_2$, Phys. Rev. Lett. **83**, 2262 (1999).
[28] T. McKay, B. O'Brien, E. Calius, and I. Anderson, in *Electroactive Polymer Actuators and Devices (EAPAD) 2012*, Vol. 8340 (International Society for Optics and Photonics, 2012) p. 83401Y.
[29] T. McKay, B. O'Brien, E. Calius, and I. Anderson, Self-priming dielectric elastomer generators, Smart Mater. Struct. **19**, 055025 (2010).
[30] R. D. James and Z. Zhang, in *Magnetism and Structure in Functional Materials*, Springer Series in Materials Science, Vol. 9, edited by A. Planes, L. Manõsa, and A. Saxena (Springer-Verlag, Berlin, 2005) p. 159–175.
[31] R. Zarnetta, R. Takahashi, M. L. Young, A. Savan, Y. Furuya, S. Thienhaus, B. Maaß, M. Rahim, J. Frenzel, H. Brunken, *et al.*, Identification of quaternary shape memory alloys with near-zero thermal hysteresis and unprecedented functional stability, Adv. Funct. Mater. **20**, 1917 (2010).
[32] Y. Song, X. Chen, V. Dabade, T. W. Shield, and R. D. James, Enhanced reversibility and unusual microstructure of a phase-transforming material, Nature **502**, 85 (2013).
[33] X. Chen, Y. Song, V. Dabade, and R. D. James, Study of the cofactor conditions: Conditions of supercompatibility between phases, J. Mech. Phys. Solids **61**, 2566 (2013).
[34] C. Chluba, W. Ge, R. L. de Miranda, J. Strobel, L. Kienle, E. Quandt, and M. Wuttig, Ultralow-fatigue shape memory alloy films, Science **348**, 1004 (2015).
[35] D. Zhao, J. Liu, X. Chen, W. Sun, Y. Li, M. Zhang, Y. Shao, H. Zhang, and A. Yan, Giant caloric effect of low-hysteresis metamagnetic shape memory alloys with exceptional cyclic functionality, Acta Mater. **133**, 217 (2017).
[36] H. Gu, L. Bumke, C. Chluba, E. Quandt, and R. D. James, Phase engineering and supercompatibility of shape memory alloys, Mater. Today **21**, 265 (2018).
[37] T. Wang, A. Prakash, Y. Dong, T. Truttmann, A. Bucsek, R. James, D. D. Fong, J.-W. Kim, P. J. Ryan, H. Zhou, *et al.*, Engineering $SrSnO_3$ phases and electron mobility at room temperature using epitaxial strain, ACS Appl. Mater. Interfaces **10**, 43802 (2018).
[38] Y. G. Liang, S. Lee, H. S. Yu, H. R. Zhang, L. A. Bendersky, Y. J. Liang, P. Y. Zavalij, X. Chen, R. D. James, and I. Takeuchi, Tuning the Hysteresis of a Metal-Insulator Transition via Lattice Compatibility, arXiv:1905.01398 (2019).
[39] C. B. Sawyer and C. H. Tower, Rochelle salt as a dielectric, Phys. Rev. **35**, 269 (1930).